HHS Public Access

Author manuscript

Cell Syst. Author manuscript; available in PMC 2016 July 29.

Published in final edited form as:

Cell Syst. 2015 July 29; 1(1): 25–36. doi:10.1016/j.cels.2015.06.002.

The AXL Receptor is a Sensor of Ligand Spatial Heterogeneity

Aaron S. Meyer[1,2,*], **Annelien J.M. Zweemer**[1,2], and **Douglas A. Lauffenburger**[1,2,*]

[1]Koch Institute for Integrative Cancer Research, Massachusetts Institute of Technology, Cambridge MA 02139

[2]Department of Biological Engineering, Massachusetts Institute of Technology, Cambridge MA 02139

Abstract

The AXL receptor is a TAM (Tyro3, AXL, MerTK) receptor tyrosine kinase (RTK) important in physiological inflammatory processes such as blood clotting, viral infection, and innate immune-mediated cell clearance. Overexpression of the receptor in a number of solid tumors is increasingly appreciated as a key drug resistance and tumor dissemination mechanism. Although the ligand-receptor (Gas6-AXL) complex structure is known, literature reports on ligand-mediated signaling have provided conflicting conclusions regarding the influence of other factors such as phosphatidylserine binding, and a detailed, mechanistic picture of AXL activation has not emerged. Integrating quantitative experiments with mathematical modeling, we show here that AXL operates to sense local spatial heterogeneity in ligand concentration, a feature consistent with its physiological role in inflammatory cell responses. This effect arises as a result of an intricate reaction-diffusion interaction. Our results demonstrate that AXL functions distinctly from other RTK families, a vital insight for envisioned design of AXL-targeted therapeutic intervention.

Introduction

TAM receptors are an RTK family, comprised of AXL, Tyro3, and MerTK, that bind the ligands Gas6 and protein S (Linger et al., 2008; Stitt et al., 1995). These receptors have attracted considerable interest in the past decade as a potential therapeutic target in a wide range of cancers. While mutations driving oncogenesis have not been identified and overexpression in the bulk tumor is typically not striking, in solid tumors overexpression of AXL in a subpopulation of cells has strongly coincided with metastatic capacity, invasiveness *in vitro*, and resistance to targeted therapies (Gjerdrum et al., 2010; Holland et al., 2010; Hutterer et al., 2008; Thomson et al., 2011; Zhang et al., 2008; 2012). Therapeutic AXL inhibitors have shown promising results in combination with other targeted or standard therapies, and have potently blocked metastasis (Gjerdrum et al., 2010; Holland et al., 2010;

*Correspondence to: lauffen@mit.edu (D.A.L.), a@ameyer.me (A.S.M.).

Author contributions: A.S.M. and D.A.L. designed the experiments. A.S.M. and A.J.M.Z. performed the experiments. A.S.M., A.J.M.Z. and D.A.L. wrote the manuscript.

Kariolis et al., 2014). Even after dissemination, targeting the distinct population of AXL-expressing cells while simultaneously targeting the bulk tumor with standard treatments may considerably extend patient survival (Allen, 2013; Gupta et al., 2011). MerTK and Tyro3 have separately been identified as therapeutic targets in acute myeloid leukemia, acute lymphoblastic leukemia, glioblastoma, melanoma, non-small cell lung carcinoma, and thyroid cancers, with more consistent patterns of overexpression (Graham et al., 1994; 2006; Lee-Sherick et al., 2013).

Therapeutically targeting the TAM receptors holds considerable promise and was initially motivated in part by the viability of knockout animals (Lu and Lemke, 2001; Lu et al., 1999). However, further study has uncovered important function of the receptors in diverse processes, cautioning against overly broad therapeutic manipulation. As the retinal pigment epithelium and Sertoli cells within the testes utilize TAM receptors for clearance of cellular debris, inhibition leads to sterility and blindness (Burstyn-Cohen et al., 2012; Chen et al., 2009b; Lu et al., 1999; Prasad et al., 2006). The most studied effects of TAM knockout have been in the immune system, where signaling from the receptors couples clearance of cell debris to negative regulation of the innate immune system (Carrera Silva et al., 2013; Lemke and Rothlin, 2008; Rothlin et al., 2007). One of the striking phenotypes of TAM triple knockout mice is widespread accumulation of apoptotic cell debris (Scott et al., 2001). Thus, it is perhaps not surprising that an effect of TAM knockout is development of autoimmune disorders, though it is unclear whether this is due to accumulation of cross-presented auto-antigen, reduced negative regulation, or both (Lu and Lemke, 2001). Some viruses in fact take advantage of TAM signaling using host-derived phosphatidylserine (PtdSer)-exposed membranes (which bind TAM ligand) to delay the immune response (Bhattacharyya et al., 2013). Because of these roles for the TAM family, approaches to manipulate endogenous TAM signaling in immune cells, if unwanted therapeutic side effects can be avoided, is a promising avenue via which to modulate the cancer immune response (Paolino et al., 2014). Indeed, blocking just *host* TAMs can potently inhibit metastasis in murine breast, melanoma, and colon cancer models (Cook et al., 2013).

While a great deal is known from genetic and structural studies, study of these receptors is severely limited currently by poor understanding of the relevant activation mechanisms (Figure 1A) (Sasaki et al., 2006). The TAM ligands Gas6 and protein S both bind PtdSer, and many studies have highlighted the importance of this interaction to activation of TAM receptors, though the exact means by which information is transduced from lipid to receptor via ligand is controversial (Dormady et al., 2000; Hall et al., 2002; Hasanbasic et al., 2005; Rajotte et al., 2008; Stenhoff et al., 2004; Yanagita et al., 1999). Earlier work identified PtdSer as an important factor to TAM activation, although it concluded that interaction between the ligand and receptor was entirely dependent upon lipid interaction, which has proven to not be the case (Nakano et al., 1997; Tanabe et al., 1997). More recent work has revisited the influence of PtdSer binding, showing that its effect is not due to a change in receptor-ligand association, and depends strongly on the spectrum of TAM receptors expressed, but has come to somewhat conflicting conclusions regarding which contexts require PtdSer for robust activation (Lew et al., 2014; Tsou et al., 2014). Studies to date have relied on stimulation with PtdSer and TAM ligand either with or without the ability to

bind PtdSer, in doing so ignoring the influence of autocrine ligand and PtdSer sources. The absence of a quantitative and mechanistic understanding of TAM receptor activation is the likely source of seemingly conflicting conclusions, and prevents not only rational targeting of the receptors but also understanding their role in diverse physiological processes.

To improve our understanding of AXL signaling, we construct and validate a reaction model of receptor-ligand engagement, trafficking, and activation. Using combined simulation and experimental validation, we demonstrate that AXL robustly senses local regions of ligand stimulation, strongly dominating over uniform ligand presentation. We show that autocrine ligand strongly influences receptor response, and that kinetic measurement is absolutely necessary to capture the relative signaling capacity of treatment conditions. Specific sensing of ligand spatial distribution is a critical feature for function of TAM receptors, particularly in sensing cellular debris. This elegant higher-order interaction between reaction and diffusional processes within an RTK emphasizes the importance of our combined experimental and modeling approach to understand the intricately patterned extracellular environment.

Results

Complexity of the AXL Response to Ligand

To investigate the basis for the complex and, at times, confounding published data on ligand-induced AXL signaling, we examined a panel of AXL expressing cancer cell lines by quantitative measurement of their dynamic response to Gas6 treatment using anti-AXL antibodies bound to beads. AXL comprised >95% of TAM receptor in the AXL-positive cell lines used (Figure S1A). To ensure the specificity of our bead-based activation quantitation, we measured receptor phosphorylation upon transfection with either full or kinase dead AXL in MDA-MB-453 cells lacking endogenous AXL expression, as well as knocked down AXL expression in MDA-MB-231 cells that do express AXL (Figure S1A & S1B).

Next, we treated a panel of cancer cell lines overexpressing AXL with varying doses of Gas6 and measured their dynamic response to stimulation (Figure S1); A549 cell line behavior is featured as a leading example (Figure 1B–E). Depending upon the cell line, Gas6-elicited AXL phosphorylation displayed either a transient peak (< 5 min) that rapidly returned to near-baseline levels or a monotonic increase in phosphorylation at high doses with relatively little response to lower doses of ligand (Figure 1B & S1C). At longer times, Gas6 stimulation could induce up to an eight-fold increase in the fraction of activated receptor (Figure S1D), ~3-fold in A549 cells (Figure 1C). Notably, the magnitude of transient responses did not correspond to those at longer times (Figure 1B, 1C, S1C & S1D). These dynamics of response are strikingly distinct from ErbB and other known RTK signaling paradigms in which receptor activation occurs very rapidly and robustly, with a straightforward relationship with respect to receptor and ligand concentrations at short and long timescales (Chen et al., 2009a; Kim et al., 2011; Kleiman et al., 2011). Application of the AXL activating antibody AF154 produced a rapid and strong phosphorylation response, confirming that the complex responses to Gas6 are a feature of AXL ligand-dependent ectodomain regulation (Figure S1E).

In total, we observed that AXL displayed unusual activation kinetics, suggesting a more complex relationship between receptor abundance and ligand concentration than observed for other, well-characterized ligand-receptor systems. Specifically, the AXL response to Gas6 lacks a uni-modal relationship to ligand concentration and displays differing responses on distinct timescales. These data highlight the importance of quantitative, dynamic measurements as these complex responses indicate any dose response relationship is highly dependent upon the duration of the assay and cellular system.

Gas6-Phosphatidylserine Interaction is Essential to Robust Long-Term AXL Phosphorylation

Gas6 interaction with PtdSer via its Gla domain (Figure 1A) has been reported as essential for robust activation of AXL (Lew et al., 2014). We hypothesized that contribution of the PtdSer interaction may confound simple interpretation of the activation kinetics we observed.

To examine the contribution of PtdSer interaction to autocrine activation of AXL, we treated four cancer cell lines with warfarin, which blocks γ-carboxylation of the Gas6 Gla domain and thus Gas6-PtdSer interaction. In each case, treatment with warfarin largely inhibited Gas6 γ-carboxylation, corresponding to no change or a decrease in AXL phosphorylation (Figure S2A & S2B). Concomitant changes in trafficking occur with inhibition of any RTK, and we found it necessary to measure total AXL abundance as well to fully capture the effect of warfarin (Figure S2A). Importantly, we still measured AXL phosphorylation in the presence of warfarin, and a different effect upon siRNA-mediated knockdown of Gas6, indicating that PtdSer interaction is not strictly essential for activation (Figure S2A). The increase in total AXL abundance with BT-549 might occur owing to a reduction in phosphorylation-dependent trafficking, while the decrease in AXL abundance with U87 may suggest that PtdSer interaction partially reduces the rate of receptor clearance (Figure S2A).

Next, we utilized Gas6 lacking the Gla domain (ΔGla Gas6), combined with warfarin pretreatment, to entirely eliminate the contribution of Gas6-PtdSer interaction (Kariolis et al., 2014). We then measured phosphorylated, total, and surface AXL abundance in A549 cells over a range of ΔGla Gas6 concentrations at one and four hours after stimulation (Figures 1D). While phosphorylated and surface receptor abundance were not significantly changed by increasing amounts of ΔGla Gas6, we did observe an increase in total receptor abundance (Figure 1D, Student's t-test, $p < 0.05$). To examine the potential for a distinct transient response, we stimulated A549 cells with 1.25 nM ΔGla Gas6 after warfarin pretreatment. Surprisingly, we observed a similar response to full length Gas6 on short (< 5 min) timescales (Figure 1E). Thus, high concentrations of Gas6 in the absence of PtdSer interaction can be in fact inhibitory of receptor activation on longer timescales, and generalization of this contribution of PtdSer to either simply "activating" or "inhibitory" is an oversimplification of a complex dynamic response (Lew et al., 2014; Tsou et al., 2014).

A Reaction Model of AXL Signaling Integrates Structural and Kinetic Understanding

To interpret our measurements in a mechanistic manner, we used a PtdSer-independent reaction model of AXL signaling. We assembled a kinetic differential equation model of

receptor-ligand binding, dimerization, and activation, incorporating current structural understanding of TAM ligand binding (Figure 2A). TAM receptor ligand bridges two receptors with asymmetric affinity for each in a mirrored arrangement (Sasaki et al., 2006). Receptor trafficking was extrapolated from knowledge of other receptor tyrosine kinase families (French and Lauffenburger, 1997; Monast et al., 2012). Briefly, new receptor synthesis occurs at a constant rate, endocytosis occurs at both an activation-dependent and -independent rate, and recycling/degradation occur at set rates with a sorting fraction determining fate for each species dependent upon activation state (Figure 2B). A_0, A_1, A_2, and A_{12} represent monomeric AXL with Gas6 bound nowhere, at the high affinity site, at the low affinity site, or at both sites, respectively (Figure 1A). D_1 and D_2 represent dimers formed by bridging receptors via one or two ligands, respectively. We measured minimal shedding of AXL (0.16% ± 0.03% that of cell-associated receptor after 24 hrs in A549), and so disregarded it as a mechanism of negative regulation.

With a model for AXL activation, we then sought to identify the rates of various binding reactions that could produce our observations for ΔGla Gas6, again featuring the A549 cell line as a central example (Figure 2C–E). We simulated our model across thousands of independent runs and calculated its fit to the ΔGla Gas6 A549 data, optimizing the fit of the remaining 11 parameters using direct search (Audet et al., 2008). Our model was able to broadly capture our measurements of A549 cell stimulation with ΔGla Gas6 in the absence of PtdSer interaction (Figure 2C), as well as in U87 cells as a second line (Figure S3). As multiple combinations of parameters were able to fit our measurements, we considered all good fits simultaneously to ensure robustness of our model interpretation. Examining each set of parameters within 5% likelihood of the optimally fit parameter set revealed that many parameters were in fact partially identifiable, such that many parameters only fit within a limited range (Figure 2D). For example, the influence of autocrine Gas6 was absolutely essential to fitting the observed responses, and the affinity of the receptor dimerization reactions (k_{f1}) was constrained within a subset of the allowed parameter range. The importance of autocrine Gas6 is perhaps trivially evident, since some amount of phosphorylation exists in A549 cells before exogenous stimulation (Figure 1D). Experimental evidence does not yet exist for whether the D_1 species is an active form of AXL; however fitting significantly selected it as a phosphorylated species (Figure 2E). This is consistent with our observation that the AXL-activating antibody AF154, which dimerizes the receptor but surely does not do so in the exact conformation of species D_2, can robustly produce receptor phosphorylation (Figure S1E).

Reaction Model Identifies Local Receptor Concentration as Limiting to Robust Response

With a model capturing the effects of ΔGla Gas6, we then sought to understand parameters that might influence receptor activation, particularly as RTK activation upon stimulation is typically 100-fold or greater in magnitude. We individually varied each fit non-trafficking parameter within 1000-fold of its value, for each set of optimal fits (Figure 3A). Each parameter set agreed that increasing the forward rate of receptor dimerization (k_{f1}) should increase the amount of phosphorylated receptor observed (Figure 3A). This suggests that receptor dimerization is a limiting step to activation of AXL regardless of the Gas6

concentration, and that factors increasing the local receptor concentration (thus increasing the forward dimerization rate) would lead to a Gas6-mediated response.

With a fit for the parameters characterizing ligand binding, we additionally sought to understand the ligand occupancy of each binding site over a range of ligand concentrations at equilibrium. The measured affinity of Gas6-AXL binding via the Ig1 domain is exceptionally high, and nearly all sites are bound at all doses of Gas6 used (Figure 3B). Model fits of Ig2 domain affinity were consistent with previous measurements of Gas6-AXL affinity measurements in the presence of Ig1-interaction mutants (Sasaki et al., 2006), and suggest that the domain is almost entirely unbound based on the bulk concentration of ligand alone (Figure 3B). The range of Gas6 concentrations in which we observed some accumulation of total AXL overlapped with the range at which some fraction of Ig2 began to be bound, suggesting that bulk Ig2 occupancy may explain this inhibition observed, since by far the predominant form of AXL on the cell surface would be A_1 (bound only at Ig1) and AXL bound at both Ig1 and Ig2 (A_{12}) would be inhibited from dimerization with this species. Thus, very high uniform concentrations of Gas6 may be in fact inhibitory, due to soluble ligand binding the Ig2 domain and thus preventing dimerization.

We further hypothesized that PtdSer interaction may drive AXL activation through relocalization of ligand to localized regions of the cell surface, corresponding to an effective increase in the rate of receptor dimerization. To more directly test this, we extended our model to account for spatial heterogeneity and diffusion of receptor, via finite differencing (Figure 3C). We created a radially symmetric region of interest (meant to represent a small portion of the cell surface), in which the concentration of Gas6 may be varied to be more uniform or alternatively concentrated in the center (Figure 3D). Diffusion is the only process defining spatial scale, and so was defined in units of the region's radius. In contrast to the homogeneous model, local stimulation was predicted to cause much stronger and sustained local receptor phosphorylation (Figure 3E) and in fact greater total receptor phosphorylation (Figure 3F). By investigating the components of the model, we determined that this increased activity corresponded to an increase in abundance of D_1 and D_2 (dimers with one or two ligands bound), and A_0 (entirely unbound receptor) (Figure 3F). Concurrently, this shift led to a decrease in A_1, A_2, and A_{12} (receptor with ligand bound at Ig1, Ig2, or both sites). Thus, our model predicts that localized presentation of ligand may drive AXL activation, even in the absence of changes upon spatially uniform stimulation.

Autocrine Phosphatidylserine Interaction Drives Punctate AXL Localization

The phenotypes observed in TAM knockout mice suggest that physiological signaling by these receptors principally arises from engagement of ligand immobilized on PtdSer-presenting surfaces, such as apoptotic cell debris, viral envelopes, and photoreceptor outer segments (Bhattacharyya et al., 2013; Lemke and Rothlin, 2008). Presentation of ligand immobilized on such surfaces would likely limit presentation of ligand to a restricted portion of the cell surface. We hypothesized that this might be a mechanism of increasing local receptor concentration using the exceptionally high affinity of Ig1. Higher local receptor concentration would exactly correspond to higher effective dimerization rates in our model,

as these parameters are the only rates influenced by receptor density. Thus our model predicts that local receptor density would directly lead to activation.

Indeed, immunofluorescence of two cell lines with autocrine activation of AXL revealed punctate staining of the receptor on the cell surface, and that this localization was ablated upon warfarin treatment (Figure 4A). While similar total staining for AXL was observed in both cell lines with warfarin treatment, there was a complete removal of dense receptor clusters (Figure 4B). Examination of the distribution of receptor densities showed a shift in receptor distribution to regions of lower receptor density (Figure 4C). Importantly, a change in receptor-ligand interaction was not observed with warfarin treatment, indicating warfarin-associated activity changes are not a consequence of changes in the amount of receptor-associated Gas6 (Figure 4D).

A Biphasic Relationship to Lipid Concentration Validates the Importance of Ig1-Driven Receptor Localization

We lastly tested, through a variety of experiments, that PtdSer-dependent AXL activity requires Ig1-mediated localization of AXL. First, we utilized 0.25 nM Gas6 to ensure that nearly all Ig1 but few Ig2 binding sites were occupied (Figure 3B) (Sasaki et al., 2006). Stimulating with just Gas6 resulted in essentially no change in receptor phosphorylation, as observed before (Figure 5A, Figure 1B & Figure S1C). However, exogenous addition of PtdSer-containing vesicles could increase AXL phosphorylation, and this was synergistically increased by addition of this low concentration of Gas6 (Figure 5A). Importantly, addition of PtdSer did not affect the amount of cell-associated Gas6 (Figure 5B). Next, we wished to test that receptor clustering, and not PtdSer interaction itself, was driving PtdSer interaction-mediated signaling. We did this in BT-549 cells, which owing to their 5-fold lower AXL expression (Figure S1A) and high degree of autocrine-mediated clustering (Figure 4B) should be highly dependent upon localized receptor for signaling. Indeed, ΔGla Gas6 provided a response upon stimulation, but only if autocrine Gas6-PtdSer interaction was present to localize the receptor (Figure 5C).

The contribution of PtdSer in terms of localizing AXL and interacting with Gas6 may be discriminated at sufficiently high concentrations of lipid, in which sufficient lipid is present so as to completely cover the cell surface (Figure 5D). At low concentrations of lipid, receptor preferentially partitions into regions of PtdSer interaction leading to a high local receptor density and driving receptor dimerization and activation. At high concentrations of lipid, even though receptor still partitions into regions of PtdSer interaction preferentially, this does not result in a high local receptor density. More specifically, observing that the relationship between local receptor density and activity is roughly proportional (Figure 3A), and that clusters contain roughly 5-fold more AXL than the surrounding cell surface (Figure 4A–C), we can specifically predict the relationship between AXL phosphorylation and lipid concentration for a constant concentration of Gas6. We again utilized a low concentration of Gas6, varying the concentration of stimulated lipid, and indeed observed a biphasic (increasing, then decreasing) relationship between lipid concentration and AXL phosphorylation (Figure 5E). This points to changes in AXL localization giving rise to the effect of Gas6-PtdSer interaction predominantly, rather than a conformational change due to

PtdSer interaction itself. Indeed, upon coupling Gas6 to polystyrene beads we could observe spots of intense phosphotyrosine staining dependent upon surface presentation of the ligand, suggesting that lipid is dispensable in the presence of another receptor localization mechanism (Figure 5F).

Discussion

The importance of PtdSer interaction to robust activation of TAM receptors has been appreciated for almost two decades, and yet a molecular understanding of this effect has not developed (Nakano et al., 1997; Tanabe et al., 1997). Our combined experiment/modeling study here provides a quantitative, mechanistic understanding of TAM signaling, and in doing so provides essential information for specific targeting of TAM signaling during both dysregulation and normal function (Figure 6). As all three TAM receptors are expected to bind both Gas6 and Protein S in a similar fashion, the methods employed here should be applicable to understanding signaling in many diverse contexts in which TAM signaling plays a role. The fact that blocking PtdSer interaction has distinct effects dependent upon the cell line used clearly emphasize the need for mechanistic, molecular understanding of TAM receptor activation, and that PtdSer does not have a simply activating or inactivating role (Figures 1B, 1E & 5E). Future studies, utilizing engineered vesicular constructs with specific properties, will be necessary to exactly define conditions of optimal TAM receptor activation.

In essence, synergy upon local stimulation is driven by asymmetry between binding sites in the affinity of ligand for receptor (Figure 3B). While most high affinity sites (Ig1) are constitutively occupied with ligand, the low affinity site (Ig2) is of insufficient affinity to drive dimerization of receptor. Localized presentation of ligand however, paired with diffusional sampling of receptor within the cell surface, allows the high affinity site Ig1 to drive relocalization of receptor such that patches of ligand also have very high concentrations of receptor. These local regions of increased ligand and receptor concentration promote binding at the low affinity site Ig2 for ligands already bound at the high affinity site Ig1. Importantly, simply raising the concentration of ligand further does not have the same effect, and in fact acts as a competitive inhibitor of receptor activation for certain ligand concentrations, since receptor activation requires pairing of complementarily bound/unbound receptors (Figure 2C).

Local patches of stimulation not only have a locally higher concentration of ligand, but diffusional sampling of the receptor followed by binding results in a higher local concentration of receptor, shifting the behavior of the system. The passive, specific contrast sensor this creates is vital to the normal physiological role of AXL as a trigger for phagocytic uptake of cellular debris. Whereas other RTK ligands can provide localized chemotactic cues, this particular system more exclusively permits AXL-expressing cells to express Gas6 and only trigger AXL activation when the ligand is trapped by PtdSer-presenting surfaces (Figure 5A). In contrast to chemoattractive cues, which arise through paracrine communication, the targets of TAM signaling need not synthesize growth factor. Through this system, a phagocytic cell can synthesize all the components needed for RTK activation including growth factor, and then phosphatidylserine exposure on the target debris

can provide the specific relocalization cue for activation. Synthetic circuits have been previously designed for detection of input discontinuities, to the exclusion of overall input magnitude, but have so far relied upon opposing influence of a locally activating input and diffusing negative regulator (Tabor et al., 2009). TAM signaling in contrast relies upon the higher order effects arising from diffusion of the receptor itself to create such a system in the absence of a separate diffusible negative regulator.

In the context of cancer therapy, our results suggest multiple mechanisms exist for modulating AXL activity within the tumor environment. Tumor cells may take advantage of spatial ligand heterogeneity to upregulate AXL signaling, and the signaling may be directly upregulated by this mechanism through phosphatidylserine exposure upon chemotherapeutic-induced apoptosis (Dunne et al., 2013). AXL expression in tumor cells may not only sequester PtdSer-presenting debris on the tumor cell surface, but also cause juxtacrine signaling upon interaction with TAM-expressing immune cells to block immunosurveilance (Paolino et al., 2014). While true cancer cell-specific targeting of AXL signaling is likely impossible, carefully engineered Gas6 binding mutants may show some specificity for dysregulated signaling, important given recent reports of negative consequences for broad TAM inhibition (Bosurgi et al., 2013). Specifically, our modeling identifies that Ig2-Gas6 binding is both relatively weak and yet required for both PtdSer-dependent and PtdSer-independent signaling, and therefore may represent a potent site of competitive inhibition (Figure 3B). More practically, study of AXL signaling has been limited by seemingly limited responses to ligand stimulation, sometimes attributed to ligand quality. Our model and quantitative analysis identifies conditions of robust AXL response, and integrates understanding of receptor function to show soluble ligand stimulation as typically performed is not the representative activation mechanism, and that localized receptor activity is likely to be most important to AXL function. Modulating TAM signaling with improved knowledge of MerTK and Tyro3 as well, both as a marker for apoptotic clearance and as a negative regulator of the immune response, holds immense promise in modulating the cancer immune response (Lemke and Rothlin, 2008; Paolino et al., 2014).

More generally, kinetic modeling provides a framework for elucidation of many complex aspects of RTK signaling and integration of extant knowledge. While ligand presentation is intricately controlled within the *in vivo* environment, such as by growth factor binding to fibrillar matrix, reaction-diffusion interactions have not been extensively identified (Casaletto and McClatchey, 2012). Beyond PtdSer, other factors in the extracellular environment may be able to relocalize TAM receptors in a similar manner by binding to ligand or receptor, and thus potently activate the receptors. Other receptors, even if mostly responsive to ligand concentration, are still likely to be modulated in important ways by localized presentation of ligand. These complex effects will only be understood through detailed mechanistic modeling due to the experimental difficulty modulating and measuring these effects. Ligand concentration is only one property of the extracellular environment useful for measurement, and we anticipate future investigations will reveal similarly elegant sensing solutions designed by natural selection.

Materials and Methods

Reagent preparation & cell culture

MDA-MB-453, SKBR3, MDA-MB-231, A549, BT-549, A172, MCF7 and U87 cells were obtained from ATCC. All cells were grown in DMEM supplemented with 10% FBS and antibiotics, except for BT-549 cells, which were grown in RPMI-1640 with 10% FBS and antibiotics. γ-carboxylated Gas6 purified from an NS0 culture in the presence of vitamin K was obtained from R&D Systems. A Gas6 mutant containing only the Laminin G-like domains and part of the last EGF domain was graciously provided by the Cochran lab (Kariolis et al., 2014; Sasaki et al., 2006). Warfarin (Sigma-Aldrich) was added where indicated 24 hrs prior to analysis at 100 μg/mL, along with new media. All ELISA measurements were performed in multiplexed fashion, using individually identifiable beads (Luminex Corp). Briefly, beads were sedimented for 3 min at 10^4×g then resuspended in 80 μL of 100 mM NaH_2PO_4 pH 6.3. 10 μL of 50 mg/mL S-NHS and 10 μL of 50 mg/mL EDC were added, and the mixture was incubated with agitation for 20 min at room temperature. Beads were then pelleted and resuspended in 300 μL 50 mM HEPES pH 7.4 with 0.1 mg/mL of either AXL, MERTK, TYRO3 and Gas6 capture antibody (R&D Systems). The mixture was incubated overnight at 4°C with agitation. The next day, the beads were washed repeatedly and stored in 1% BSA in PBS. Coupling efficiency was measured using biotinylated protein G. Cells were always lysed in 50 mM Tris, 10% glycerol, 150 mM NaCl, 1% NP40 at pH 7.5 with cOmplete protease inhibitor (Roche) and phosphatase inhibitor I (Boston Bioproducts).

Quantification of receptor abundance, shedding, phosphorylation, and cell-associated ligand

For lipid stimulation, 5:3:2 w/w phosphatidylethanolamine:phosphatidylserine: phosphatidylcholine (Avanti Polar Lipids) was resuspended in L15 media with 0.35% BSA at 4 mg/mL, vortexed vigorously, then diluted to the indicated concentration. 0.25 nM Gas6 was added where indicated, and the mixture was incubated with gentle shaking for 1 hour. Cells were starved for 4 hours then treated and lysed.

Protein concentration was measured by bicinchoninic acid assay. Lysates were incubated with capture beads overnight with agitation, then washed with 0.1% Tween-20 in PBS and incubated with either detection antibodies for each TAM receptor (R&D Systems) or biotinylated 4G10 for 30 min. After washing again, beads were incubated with streptavidin-phycoerythrin for 10 min and then quantified using a FlexMap 3D (Luminex Corp). Receptor abundance was quantified by comparison to a recombinant standard (R&D Systems).

Surface abundance was measured by surface biotinylation. After treatment for the indicated time, cells were washed repeatedly with ice cold PBS then incubated at 4°C with cell impermeable sulfo-NHS-biotin for 30 min. Surface labeling was halted by lysis. Capture beads were then incubated with the lysate overnight, and the next day labeling was quantified using streptavidin-phycoerythrin.

Cell-associated ligand was measured by repeatedly washing cells with PBS and then measuring the amount of Gas6 present in the lysate. Receptor shedding was quantified by incubating cells in serum free medium in the presence of either 0 or 1.25 nM Gas6 for 24 hours, and then collecting the supernatant and cell lysate. Supernatants were clarified by centrifugation at 3000×g for 10 min to remove potential cell debris. Receptor abundance was then measured in each fraction, and adjusted by total volume to derive a total amount in the supernatant or cell lysate.

Barium citrate precipitation and AXL co-immunoprecipitation of γ-carboxylated Gas6

After cells were lysed and lysate was clarified, 18 μL of 1 M $BaCl_2$ was added per 400 μL of lysate to each sample. Samples were incubated with end over end mixing for 1 hour, and then spun at 10^4×g for 5 min at 4°C to yield a precipitated pellet. The supernatant was removed and stored separately, and then the pellet was resuspended in 0.1 $BaCl_2$ and 0.1 M NaCl in ddH_2O to wash. Each sample was again incubated with mixing at 4°C and then pelleted by centrifugation. The pellet was resolubilized in a minimal amount of 0.5 M EDTA pH 8.

For AXL-Gas6 co-immunoprecipitation, lysates were incubated with 10 μg AXL ELISA capture antibody and 50 μL pre-washed protein G agarose for 4 hrs with gentle rocking. The resin was then washed repeatedly with lysis buffer and eluted by boiling in denaturing sample buffer.

AXL was blotted using the ELISA capture antibody, and Gas6 using the ELISA detection antibody or another antibody against the ligand (Abcam, ab136249).

AXL mutant and siRNA transfection

AXL mutants were blunt-end cloned into pIRESpuro2 (Clontech) from wild-type human cDNA to create a kinase dead (K562R) mutant. 500,000 cells were seeded in 10 cm plates. The next day, cells were transfected with 10 μg DNA of each AXL mutant using 10 μL Lipofectamine in OptiMEM according to the manufacturer's instructions. Four hours post-transfection growth media was added back to the cells. After 24 hours, cells were starved 4 hours and then lysed.

For siRNA treatment, plates were transfected with 5 μL Dharmafect 4 and 125 fmol of pooled siRNA in OptiMEM, then placed back in full serum media four hours later. Two days after transfection cells were starved for 4 hours then lysed. Oligonucleotides against human transcripts were (5'-3'): siControl ON-TARGETplus Non-targeting Pool D-001810-10-05, siAXL (pooled four siRNAs) ON-TARGETplus SMARTpool siRNA L-003104-00, siGas6 (pooled four siRNAs) ON-TARGETplus SMARTpool siRNA L-009069-00.

Immunofluorescence

Coverslips were coated with 100 μg/mL collagen I in 20 mM acetic acid, then seeded with cells in the presence or absence of warfarin. Cells were fixed 24 hrs later with 4% paraformaldehyde in PHEM buffer. Fixed cells were permeabilized with 0.1% Triton X-100

and 1% BSA in PBS, then blocked 30 min using Odyssey blocking buffer (OBB; Li-Cor Corp.). The primary antibody (R&D Systems: AXL mAb, MAB154, 5 μg/mL) was incubated for 1 hour at room temperature in OBB. After washing with 1% BSA in PBS, cells were incubated with phalloidin and secondary antibodies for 1 hour and finally washed with 1% BSA in PBS.

For bead-based stimulation, Gas6 was coupled to polystyrene beads following identical methods to the capture antibodies. Coupled beads were washed six times to remove uncoupled protein. Cells were starved for 4 hr, and then beads were added and allowed to settle for the indicated amount of time. 4% PFA in PHEM buffer with phosphatase inhibitor (Boston Bioproducts) was used to fix the cells for 10 min. Immunofluorescence was performed by standard methods, with 1 μg/mL phosphotyrosine antibody (P-Tyr-100, Cell Signaling Technology).

Imaging was performed using a CARVII spinning disk confocal microscope with a 40× objective. Stacks were imaged every 1 μm, and then processed by maximum projection.

Model parameterization

AXL signaling kinetics was modeled using ordinary differential equations, and the model layout was inferred from structural understanding of ligand binding (Sasaki et al., 2006). A_0, A_1, A_2, and A_{12} indicate AXL in an unbound state, bound at the high affinity site, bound at the low affinity site, and bound at both sites, respectively. D_1 indicates the dimer species with one Gas6 molecule bridging receptors. D_2 indicates the full receptor-ligand complex with two Gas6 molecules dimerizing two receptors. Phosphorylation was assumed to occur fast, such that species abundance directly translated to phosphorylated receptor abundance (Monast et al., 2012). Dimerization of receptors to form the D_2 species was modeled as a one step reaction implicitly assuming the second binding after dimerization through the first interface was fast. As the local concentration of incompletely dimerized Gas6 would be in excess of 1 M in the intermediate state, we believe this is a suitable assumption. The forward rates of receptor dimerization were assumed to be equal. Ig1 binding rates were set according to previous measurements (Kariolis et al., 2014). The on rate of Ig2 binding, k_{fb2}, was set to 10^7 M^{-1} sec^{-1} as binding affinity is rarely governed by distinct on rates. The reverse reaction rate for dimerization reaction 1, k_{r1}, was assumed to be equal to the reverse binding rate of Ig2, k_{rb2}, as a single ligand is the sole bridge between receptors, and the off-rate of Ig2 is at least 100-fold higher than that of Ig1. Autocrine ligand was assumed to be present at a constant concentration, with stimulated ligand adding to that concentration.

$$\frac{dA_0}{dt}=k_{rb1}A_1+k_{rb2}A_2+(k_{r1}+k_{r2})D_1+k_{r3}D_2+v-(k_{f1}A_1+k_{f2}A_2+k_{f3}A_{12}+k_{fb1}G+k_{fb2}G)A_0$$

$$\frac{dA_1}{dt}=k_{fb1}GA_0-k_{rb1}A_1-k_{fb2}GA_1+k_{rb2}A_{12}-k_{f1}A_0A_1+k_{r1}D_1-2k_{f4}A_1^2+2k_{r4}D_2$$

$$\frac{dA_2}{dt}=k_{fb2}GA_0+k_{rb1}A_{12}+k_{r2}D_1+2k_{r5}D_2-(k_{rb2}+k_{fb1}G+k_{f2}A_0+2k_{f5}A_2)A_2$$

$$\frac{dA_{12}}{dt}=(k_{fb2}A_1+k_{fb1}A_2)G-(k_{rb1}+k_{rb2}+k_{f3}A_0)A_{12}+k_{r3}D_2$$

$$\frac{dD_1}{dt}=k_{r6}D_2+k_{f2}A_0A_2+k_{f1}A_0A_1-(k_{f6}G+k_{r2}+k_{r1})D_1$$

$$\frac{dD_2}{dt}=k_{f6}D_1G+k_{f5}A_2^2+k_{f4}A_1^2+k_{f3}A_0A_{12}-(k_{r3}+k_{r6}+k_{r5}+k_{r4})D_2$$

A subset of parameters was constrained due to detailed balance, as indicated in Figure 2A.

Trafficking was modeled and kinetically constrained based on understanding from other receptor tyrosine kinases (French and Lauffenburger, 1997; Monast et al., 2012). We first assumed that endocytosis and endosomal sorting of each species occurred according to phosphorylation state. A faster phosphorylation-dependent rate ($k_{int,2}$) and slower phosphorylation-independent rate ($k_{int,1}$) were included, as observed with other RTK families (Monast et al., 2012). Fluid-phase uptake of ligand was assumed to not occur as its contribution has only been observed at very high extracellular concentrations. Endosomal maturation and degradation were modeled as done previously, with no sorting of ligand. The ligand compartment was assumed to comprise 2% of cellular volume, or 10 fL per cell, and the endosomal surface area was assumed to be half that of the plasma membrane. Receptor and ligand interactions were assumed to be identical within the endosomal compartment. Trafficking was defined by:

$$\frac{dX}{dt}=-X(k_{int,1}+S_ak_{int,2})+k_{rec}(1-f)\gamma X_i$$

$$\frac{dX_i}{dt}=\frac{X}{\gamma}(k_{int,1}+S_ak_{int,2})+k_{rec}(1-f)X_i-k_{deg}fX_i$$

f is the sorting fraction for each species, which is the fractional propensity of a species to be degraded instead of recycled. As such, $f = 1$ means all of that endocytosed species is degraded and $f = 0$ means all is recycled. f is f_{else} for non-phosphorylated species and 1 for phosphorylated ones.

The model was implemented as an external library to MatLab 2013b in C++ using CVode, using the backward differentiation formula and Newton iteration, with the dense Jacobian solver (Hindmarsh et al, 2005). Integration was performed for 10000 minutes in order to

ensure the model had arrived at equilibrium in the presence of autocrine ligand before the addition of exogenous stimulus at t = 0. χ^2 values were calculated from the standard error of each measurement, for the A549 cell line, using experimental replicates. At least 1000 independent times, global optimization was performed from a random starting point using the direct search method *patternsearch* within MatLab. Multiple independent optimization trials were confirmed to converge on the same optimal fit. All code used is available as a supplement or online with further documentation for extended usage at (https://github.com/thanatosmin/AXLdiffEQ). For validation of model predictions in the U87 cell line, each parameter set was adjusted by fitting only AXL expression and autocrine Gas6 abundance to the U87 data, and then plotted over the measured values.

Spatial Modeling

Spatial modeling was performed by finite differencing on a 2D, radially symmetric geometry of radius L, integrated using CVode (Hindmarsh et al., 2005). Within the region of interest diffusion was modeled using explicit central difference approximation:

$$\frac{\delta c_{x,i}}{D_x \delta t} = \frac{-4c_{x,i} + (2 - i^{-1})c_{x,i-1} + (2 + i^{-1})c_{x,i+1}}{2\Omega}$$

where D_x is the diffusion coefficient of species x, $c_{x,i}$ is the concentration of species x at discrete position i, i is the index of each discretized point along the radius of the region of interest, and $\Omega = L^2 N^{-2}$, where N is the number of discretized points along the radius.

As diffusion is the only parameter that defines the length scale of the system, other lengths are defined in terms of L. $r = L$ was set as a closed boundary, and at $r = 0$ the solution was assumed to be finite. As such, diffusion at the boundaries was calculated to be:

$$\frac{\delta c_{x,0}}{D_x \delta t} = \frac{4}{\Omega}(c_{x,1} - c_{x,0})$$

$$\frac{\delta c_{x,L}}{D_x \delta t} = \frac{4}{\Omega}(c_{x,L} - c_{x,L-1})$$

Diffusion was selected to occur for A_0 and internal species, as Gas6 binding was assumed to reduce mobility. Reactions occurred normally throughout the region of interest unless noted otherwise. The extracellular Gas6 concentration profile was fixed as:

$$[Gas6] = 64 \cos\left(\frac{\pi r}{3L}\right)^{\sigma}$$

where σ is a “spatial inhomogeneity” parameter.

Simplified model of clustering effect

Based on the assumption that local receptor density is limiting to activation, we constructed a simplified two-compartment model in which receptor activity is related proportionally and exclusively to local receptor density. Receptor was assumed to partition between a phosphatidylserine-interacting and phosphatidylserine-absent compartment with partition coefficient *K*, with a defined fractional surface area *x* of the former compartment. The amount of phosphorylated receptor (*Y*) is thus defined as:

$$Y = b^2 x + c^2 (1 - x)$$

where *b* and *c* represent the local receptor densities of each compartment. After conservation of total receptor mass the amount of phosphorylated receptor thus becomes:

$$Y = \frac{K^2 x + 1 - x}{(Kx + 1 - x)^2}$$

We assumed $K = 5$ based on the intensities of spots observed in immunofluorescence, and experimentally determined the relationship between fractional surface coverage and lipid concentration based on the response observed.

Calculation of binding fractional occupancy

The fractional binding of each ligand-receptor interaction surface was calculated according to equilibrium binding ignoring the contributions of any trafficking or dimerization processes. Thus, the fraction of receptor unbound is defined as:

$$x = \frac{K_D}{K_D + L}$$

where L is the ligand concentration, and K_D is the ratio of the off to on rate of receptor-ligand binding.

Acknowledgments

The authors thank Shannon Hughes, Jennifer Cochran and Forest White for helpful comments, and Jennifer Cochran for the ΔGla Gas6 ligand.

Funding: NIH U54-CA112967 to D.A.L. and DP5-OD019815 to A.S.M. supported this work. Additionally, this work was partially supported by the Institute for Collaborative Biotechnologies grant W911NF-09-0001 from the U.S. Army Research Office, and the Koch Institute Support (core) Grant P30-CA14051 from the National Cancer Institute.

References

Allen B. Evolutionary dynamics of cancer in response to targeted combination therapy. eLife. 2013; 2:e00747–e00747. [PubMed: 23805382]

Audet C, Béchard V, Le Digabel S. Nonsmooth optimization through Mesh Adaptive Direct Search and Variable Neighborhood Search. J Glob Optim. 2008; 41:299–318.

Bhattacharyya S, Zagórska A, Lew ED, Shrestha B, Rothlin CV, Naughton J, Diamond MS, Lemke G, Young JA. Enveloped Viruses Disable Innate Immune Responses in Dendritic Cells by Direct Activation of TAM Receptors. Cell Host and Microbe. 2013; 14:136–147. [PubMed: 23954153]

Bosurgi L, Bernink JH, Delgado Cuevas V, Gagliani N, Joannas L, Schmid ET, Booth CJ, Ghosh S, Rothlin CV. Paradoxical role of the proto-oncogene Axl and Mer receptor tyrosine kinases in colon cancer. Proc. Natl. Acad. Sci. U.S.a. 2013

Burstyn-Cohen T, Lew ED, Través PG, Burrola PG, Hash JC, Lemke G. Genetic Dissection of TAM Receptor-Ligand Interaction in Retinal Pigment Epithelial Cell Phagocytosis. Neuron. 2012; 76:1123–1132. [PubMed: 23259948]

Carrera Silva EA, Chan PY, Joannas L, Errasti AE, Gagliani N, Bosurgi L, Jabbour M, Perry A, Smith-Chakmakova F, Mucida D, et al. T cell-derived protein S engages TAM receptor signaling in dendritic cells to control the magnitude of the immune response. Immunity. 2013; 39:160–170. [PubMed: 23850380]

Casaletto JB, McClatchey AI. Spatial regulation of receptor tyrosine kinases in development and cancer. Nat. Rev. Cancer. 2012; 12:387–400. [PubMed: 22622641]

Chen WW, Schoeberl B, Jasper PJ, Niepel M, Nielsen UB, Lauffenburger DA, Sorger PK. Input-output behavior of ErbB signaling pathways as revealed by a mass action model trained against dynamic data. Mol Syst Biol. 2009a; 5:1–19.

Chen Y, Wang H, Qi N, Wu H, Xiong W, Ma J, Lu Q. Functions of TAM RTKs in regulating spermatogenesis and male fertility in mice. Reproduction. 2009b; 138:655–666. [PubMed: 19602523]

Cook RS, Jacobsen KM, Wofford AM, DeRyckere D, Stanford J, Prieto AL, Redente E, Sandahl M, Hunter DM, Strunk KE, et al. MerTK inhibition in tumor leukocytes decreases tumor growth and metastasis. J Clin Invest. 2013; 123:3231–3242. [PubMed: 23867499]

Dormady SP, Zhang XM, Basch RS. Hematopoietic progenitor cells grow on 3T3 fibroblast monolayers that overexpress growth arrest-specific gene-6 (GAS6). Proc. Natl. Acad. Sci. USA. 2000; 97:12260–12265. [PubMed: 11050245]

Dunne PD, McArt DG, Blayney JK, Kalimutho M, Greer S, Wang T, Srivastava S, Ong CW, Arthur K, Loughrey M, et al. AXL Is a Key Regulator of Inherent and Chemotherapy-Induced Invasion and Predicts a Poor Clinical Outcome in Early-Stage Colon Cancer. Clin. Cancer Res. 2013

French AR, Lauffenburger DA. Controlling receptor/ligand trafficking: Effects of cellular and molecular properties on endosomal sorting. Ann Biomed Eng. 1997; 25:690–707. [PubMed: 9236981]

Gjerdrum C, Tiron C, Høiby T, Stefansson I, Haugen H, Sandal T, Collett K, Li S, McCormack E, Gjertsen B. AXL is an essential epithelial-to-mesenchymal transition-induced regulator of breast cancer metastasis and patient survival. Proc. Natl. Acad. Sci. USA. 2010; 107:1124. [PubMed: 20080645]

Graham DK, Dawson TL, Mullaney DL, Snodgrass HR, Earp HS. Cloning and mRNA expression analysis of a novel human protooncogene, c-mer. Cell Growth Differ. 1994; 5:647–657. [PubMed: 8086340]

Graham DK, Salzberg DB, Kurtzberg J, Sather S, Matsushima GK, Keating AK, Liang X, Lovell MA, Williams SA, Dawson TL, et al. Ectopic expression of the proto-oncogene Mer in pediatric T-cell acute lymphoblastic leukemia. Clin. Cancer Res. 2006; 12:2662–2669. [PubMed: 16675557]

Gupta PB, Fillmore CM, Jiang G, Shapira SD, Tao K, Kuperwasser C, Lander ES. Stochastic State Transitions Give Rise to Phenotypic Equilibrium in Populations of Cancer Cells. Cell. 2011; 146:633–644. [PubMed: 21854987]

Hall MO, Obin MS, Prieto AL, Burgess BL, Abrams TA. Gas6 Binding to Photoreceptor Outer Segments Requires γ-Carboxyglutamic Acid (Gla) and Ca2+ and is Required for OS Phagocytosis by RPE Cells in vitro. Experimental Eye Research. 2002; 75:391–400. [PubMed: 12387786]

Hasanbasic I, Rajotte I, Blostein M. The role of gamma-carboxylation in the anti-apoptotic function of gas6. J. Thromb. Haemost. 2005; 3:2790–2797. [PubMed: 16359517]

Hindmarsh AC, Brown PN, Grant KE, Lee SL, Serban R, Shumaker DE, Woodward CS. SUNDIALS. ACM Trans. Math. Softw. 2005; 31:363–396.

Holland SJ, Pan A, Franci C, Hu Y, Chang B, Li W, Duan M, Torneros A, Yu J, Heckrodt TJ, et al. R428, a selective small molecule inhibitor of Axl kinase, blocks tumor spread and prolongs survival in models of metastatic breast cancer. Cancer Res. 2010; 70:1544–1554. [PubMed: 20145120]

Hutterer M, Knyazev P, Abate A, Reschke M, Maier H, Stefanova N, Knyazeva T, Barbieri V, Reindl M, Muigg A, et al. AXL and growth arrest-specific gene 6 are frequently overexpressed in human gliomas and predict poor prognosis in patients with glioblastoma multiforme. Clin. Cancer Res. 2008; 14:130–138. [PubMed: 18172262]

Kariolis MS, Miao YR, Jones DS, Kapur S, Mathews II, Giaccia AJ, Cochran JR. An engineered Axl "decoy receptor" effectively silences the Gas6-Axl signaling axis. Nature Chemical Biology. 2014; 10:977–983. [PubMed: 25242553]

Kim H-D, Meyer AS, Wagner JP, Alford SK, Wells A, Gertler FB, Lauffenburger DA. Signaling network state predicts twist-mediated effects on breast cell migration across diverse growth factor contexts. Mol. Cell. Proteomics. 2011; 10 M111.008433.

Kleiman LB, Maiwald T, Conzelmann H, Lauffenburger DA, Sorger PK. Rapid phospho-turnover by receptor tyrosine kinases impacts downstream signaling and drug binding. Mol. Cell. 2011; 43:723–737. [PubMed: 21884975]

Lee-Sherick AB, Eisenman KM, Sather S, McGranahan A, Armistead PM, McGary CS, Hunsucker SA, Schlegel J, Martinson H, Cannon C, et al. Aberrant Mer receptor tyrosine kinase expression contributes to leukemogenesis in acute myeloid leukemia. Oncogene. 2013; 32:5359–5368. [PubMed: 23474756]

Lemke G, Rothlin CV. Immunobiology of the TAM receptors. Nat Rev Immunol. 2008; 8:327–336. [PubMed: 18421305]

Lew ED, Oh J, Burrola PG, Lax I, Zagórska A, Través PG, Schlessinger J, Lemke G. Differential TAM receptor-ligand-phospholipid interactions delimit differential TAM bioactivities. eLife. 2014:3.

Linger RMA, Keating AK, Earp HS, Graham DK. TAM receptor tyrosine kinases: biologic functions, signaling, and potential therapeutic targeting in human cancer. Adv. Cancer Res. 2008; 100:35–83. [PubMed: 18620092]

Lu Q, Lemke G. Homeostatic regulation of the immune system by receptor tyrosine kinases of the Tyro 3 family. Science. 2001; 293:306–311. [PubMed: 11452127]

Lu Q, Gore M, Zhang Q, Camenisch T, Boast S, Casagranda F, Lai C, Skinner MK, Klein R, Matsushima GK, et al. Tyro-3 family receptors are essential regulators of mammalian spermatogenesis. Nature. 1999; 398:723–728. [PubMed: 10227296]

Monast CS, Furcht CM, Lazzara MJ. Computational Analysis of the Regulation of EGFR by Protein Tyrosine Phosphatases. Biophys J. 2012

Nakano T, Kawamoto K, Kishino J, Nomura K, Higashino K, Arita H. Requirement of gamma-carboxyglutamic acid residues for the biological activity of Gas6: contribution of endogenous Gas6 to the proliferation of vascular smooth muscle cells. Biochem J. 1997; 323(Pt 2):387–392. [PubMed: 9163328]

Paolino M, Choidas A, Wallner S, Pranjic B, Uribesalgo I, Loeser S, Jamieson AM, Langdon WY, Ikeda F, Fededa JP, et al. The E3 ligase Cbl-b and TAM receptors regulate cancer metastasis via natural killer cells. Nature. 2014

Prasad D, Rothlin CV, Burrola P, Burstyn-Cohen T, Lu Q, Garcia de Frutos P, Lemke G. TAM receptor function in the retinal pigment epithelium. Mol. Cell. Neurosci. 2006; 33:96–108. [PubMed: 16901715]

Rajotte I, Hasanbasic I, Blostein M. Gas6-mediated signaling is dependent on the engagement of its gamma-carboxyglutamic acid domain with phosphatidylserine. Biochem. Biophys. Res. Commun. 2008; 376:70–73. [PubMed: 18760998]

Rothlin CV, Ghosh S, Zuniga EI, Oldstone MBA, Lemke G. TAM Receptors Are Pleiotropic Inhibitors of the Innate Immune Response. Cell. 2007; 131:1124–1136. [PubMed: 18083102]

Sasaki T, Knyazev PG, Clout NJ, Cheburkin Y, Göhring W, Ullrich A, Timpl R, Hohenester E. Structural basis for Gas6-Axl signalling. Embo J. 2006; 25:80–87. [PubMed: 16362042]

Scott RS, McMahon EJ, Pop SM, Reap EA, Caricchio R, Cohen PL, Earp HS, Matsushima GK. Phagocytosis and clearance of apoptotic cells is mediated by MER. Nature. 2001; 411:207–211. [PubMed: 11346799]

Stenhoff J, Dahlbäck B, Hafizi S. Vitamin K-dependent Gas6 activates ERK kinase and stimulates growth of cardiac fibroblasts. Biochem. Biophys. Res. Commun. 2004; 319:871–878. [PubMed: 15184064]

Stitt TN, Conn G, Gore M, Lai C, Bruno J, Radziejewski C, Mattsson K, Fisher J, Gies DR, Jones PF. The anticoagulation factor protein S and its relative, Gas6, are ligands for the Tyro 3/Axl family of receptor tyrosine kinases. Cell. 1995; 80:661–670. [PubMed: 7867073]

Tabor JJ, Salis HM, Simpson ZB, Chevalier AA, Levskaya A, Marcotte EM, Voigt CA, Ellington AD. A Synthetic Genetic Edge Detection Program. Cell. 2009; 137:1272–1281. [PubMed: 19563759]

Tanabe K, Nagata K, Ohashi K, Nakano T, Arita H, Mizuno K. Roles of γ-carboxylation and a sex hormone-binding globulin-like domain in receptor-binding and in biological activities of Gas6. FEBS Letters. 1997; 408:5–5. [PubMed: 9180257]

Thomson S, Petti F, Sujka-Kwok I, Mercado P, Bean J, Monaghan M, Seymour SL, Argast GM, Epstein DM, Haley JD. A systems view of epithelial-mesenchymal transition signaling states. Clin. Exp. Metastas. 2011; 28:137–155.

Tsou W-I, Nguyen K-QN, Calarese DA, Garforth SJ, Antes AL, Smirnov SV, Almo SC, Birge RB, Kotenko SV. Receptor Tyrosine Kinases, TYRO3, AXL and MER, Demonstrate Distinct Patterns and Complex Regulation of Ligand-Induced Activation. J Biol Chem. 2014 jbc.M114.569020.

Yanagita M, Ishii K, Ozaki H, Arai H, Nakano T, Kita T, Doi T. Mechanism of inhibitory effect of warfarin on mesangial cell proliferation. J. Am. Soc. Nephrol. 1999; 10:2503–2509. [PubMed: 10589688]

Zhang Y, Knyazev P, Cheburkin Y, Sharma K, Knyazev Y, Orfi L, Szabadkai I, Daub H, Keri G, Ullrich A. AXL is a potential target for therapeutic intervention in breast cancer progression. Cancer Res. 2008; 68:1905. [PubMed: 18339872]

Zhang Z, Lee JC, Lin L, Olivas V, Au V, LaFramboise T, Abdel-Rahman M, Wang X, Levine AD, Rho JK, et al. Activation of the AXL kinase causes resistance to EGFR-targeted therapy in lung cancer. Nat. Genet. 2012:1–11.

Highlights

- The dynamics of AXL receptor activation are distinct from those of other RTK families
- Spatially heterogeneous presentation of the ligand Gas6 leads to enhanced AXL response
- Localization and activation of AXL can arise from Gas6/phosphatidylserine interactions
- A diffusion-reaction model can account for the influence of phosphatidylserine

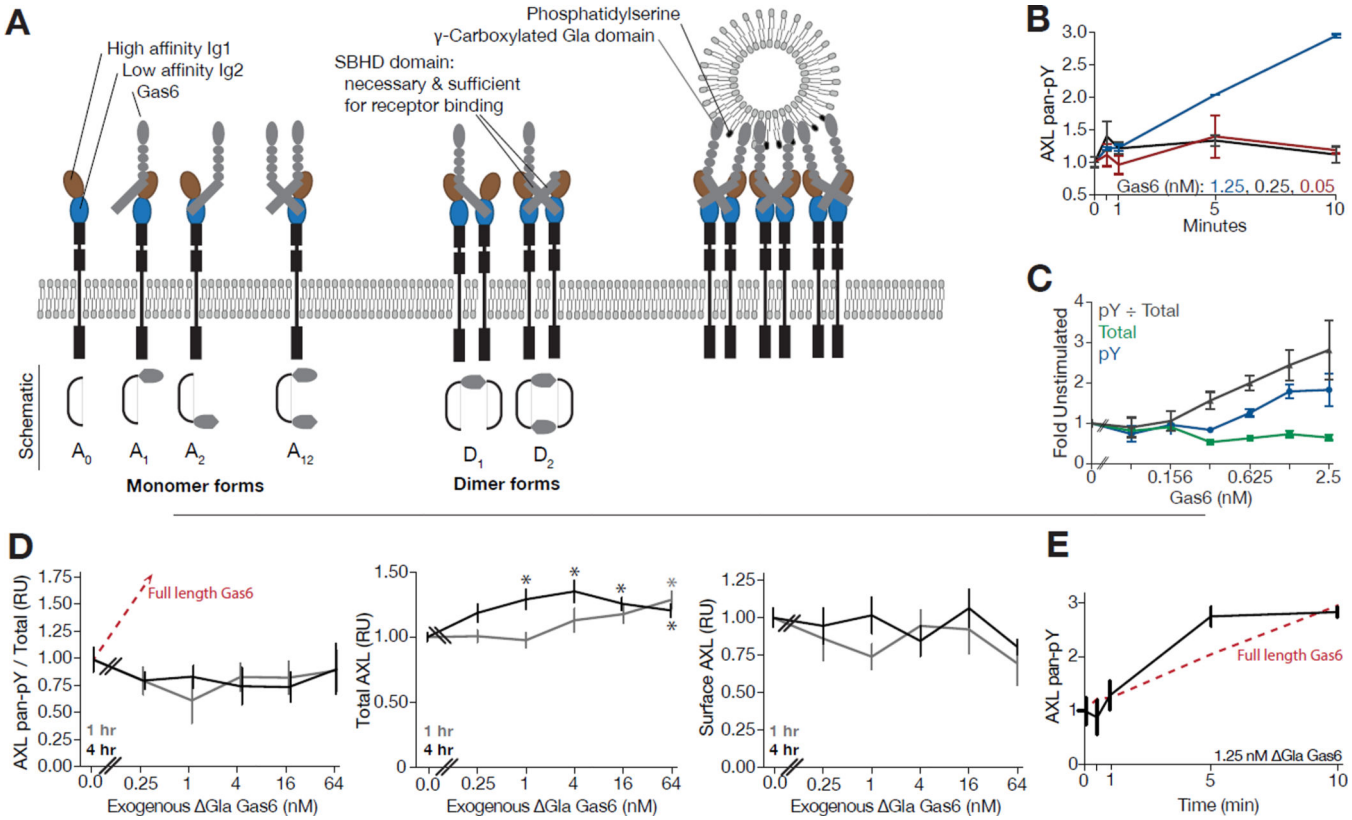

Figure 1. AXL phosphorylation response is complex, distinct across timescales, and requires PtdSer interaction for robust response

(A) Diagram of AXL-Gas6 interaction. Receptor and ligand interact through a high- (brown, Ig1) and low-affinity (blue, Ig2) binding interface. These interactions, only mediated through the SBHD domain, lead to receptor dimerization with no receptor-receptor ectodomain interactions. However, through previously unknown mechanisms, PtdSer interaction via the Gla domain is known to be important to receptor activation. The structural aspects of TAM receptor-ligand interaction are thought to be shared among all three TAM receptors and two ligands, although AXL lacks measurable binding to Protein S. (B–C) ELISA-based quantitative measurement of AXL phosphotyrosine and total abundance upon treatment with indicated concentrations of Gas6 at 0–10 min (B) or 4 hrs (C). (D) Measurement of phosphotyrosine and total AXL in warfarin-treated A549 cells upon stimulation with ΔGla Gas6 for one or four hours. Red line shows corresponding response measured upon stimulation with full length Gas6 in (C). *Significant change from untreated control (Student's t-test, $p < 0.05$). (E) Measurement of phosphotyrosine AXL in warfarin-treated A549 cells upon stimulation with 1.25 nM ΔGla Gas6 over 10 min. Red line shows corresponding response measured upon stimulation with full length Gas6 in (D). Error bars indicate standard error of triplicate measurement.

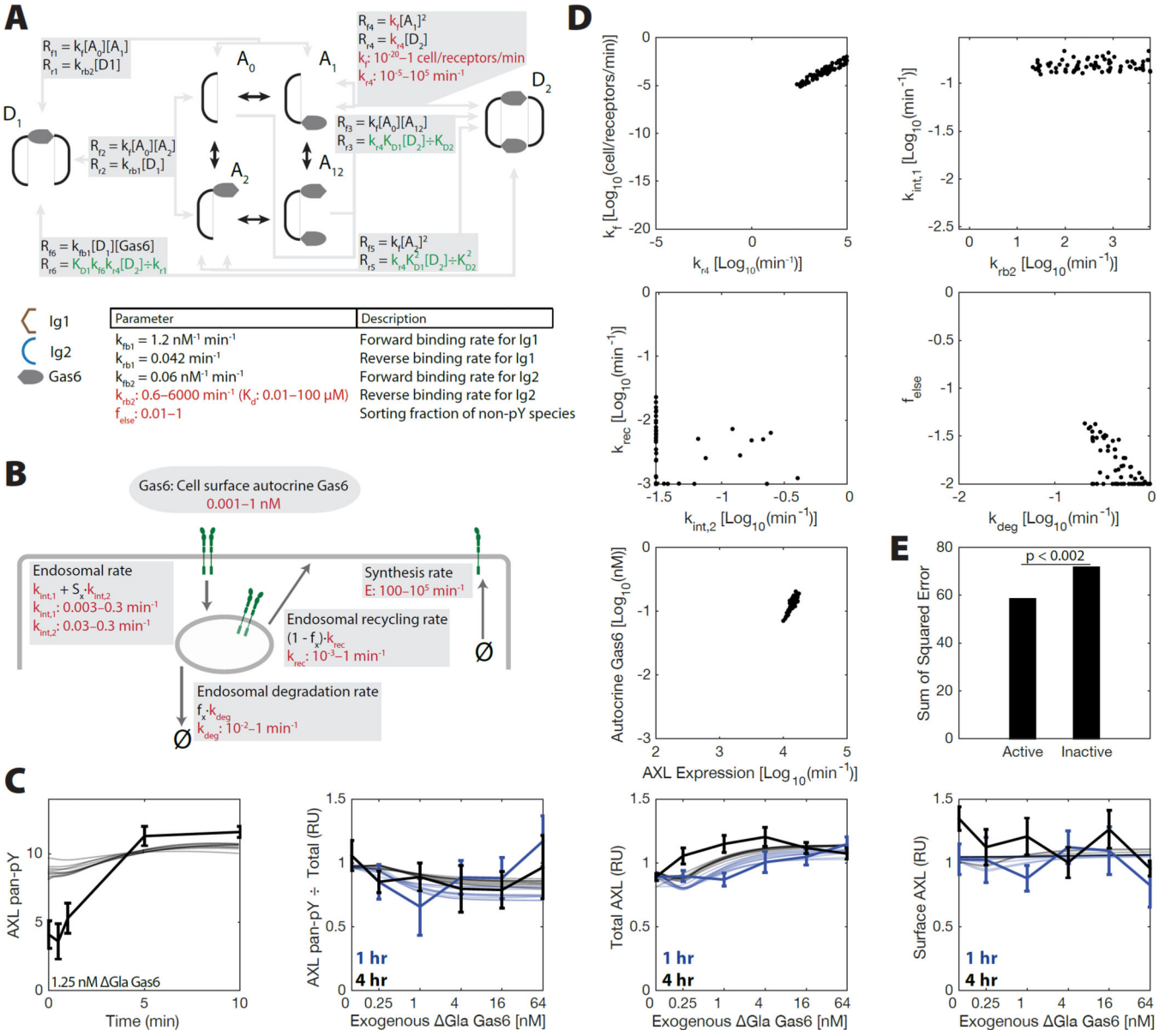

Figure 2. A reaction model of AXL signaling integrates structural and kinetic understanding

(A) Diagram of the AXL reaction model. Trafficking is not shown. Binding reactions occur identically with internalized and surface species. (B) Model of AXL trafficking. Receptor expression occurs constitutively. Endocytosis occurs at a basal and activation-dependent rate. Recycling and degradation occur at prescribed rates, with a sorting fraction to determine which occurs. f_x is 1 for phosphorylated species and f_{else} for all other species. Some parameters were fit within their indicated range (red), while others were constrained by detailed balance (green) or assumptions (black). (C) Measurements compared with simulations from all parameter fits within 5% likelihood of the optimal fit. (D) Parameter values observed in all fits with a relative likelihood within 5% that of the optimal fit. (E) Sum-of-squared error for the best-fit parameter sets in which species D_1 is either active or inactive.

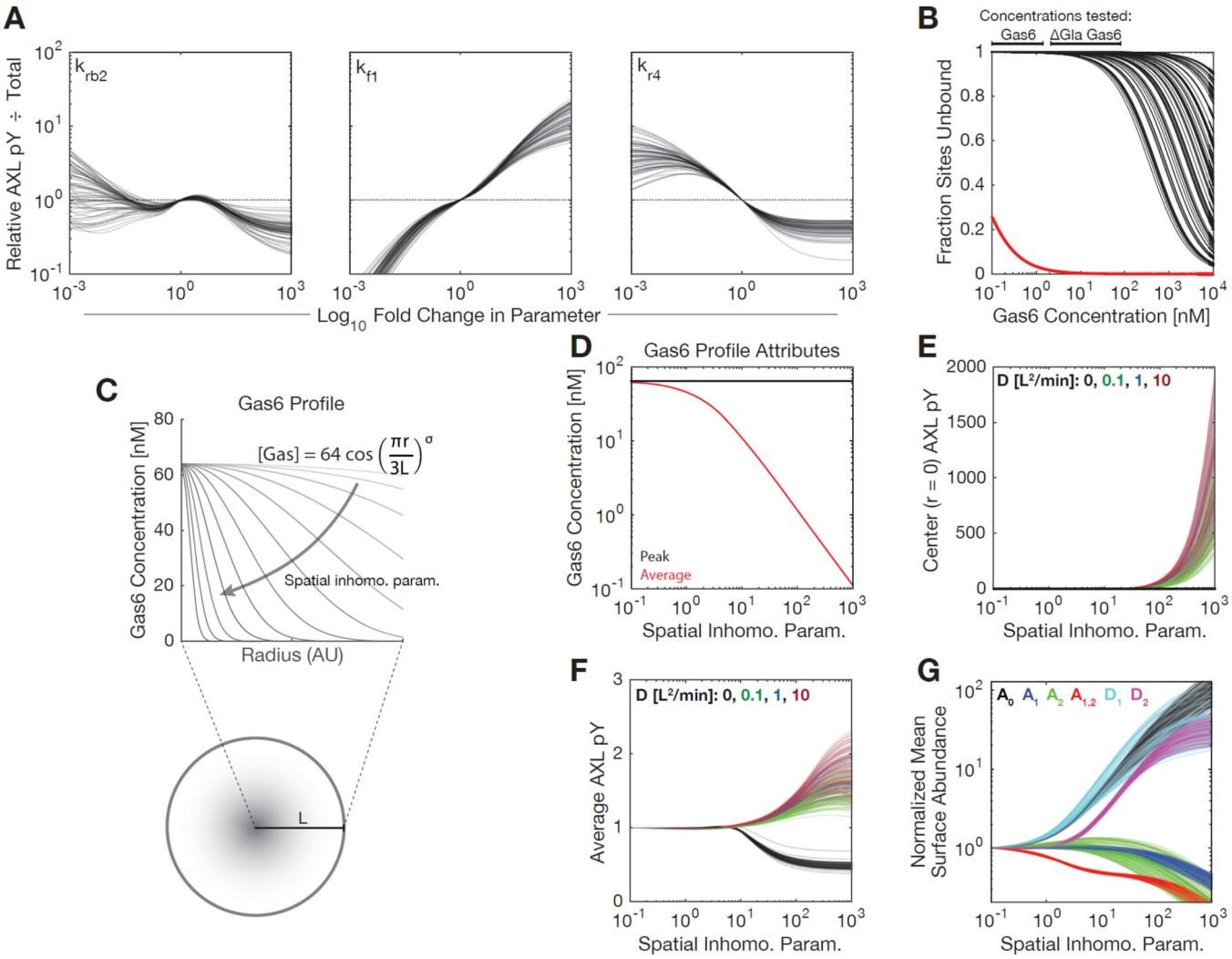

Figure 3. A PtdSer-independent and reaction-diffusion model indicate local receptor concentration is rate limiting for robust activation

(A) The relative fraction of activated receptor upon variation of each reaction parameter. Response is shown for stimulation with 10 nM Gas6 for 4 hrs. (B) Fractional vacancy of Ig1 (red) and Ig2 (black) binding sites based on fit or measured affinities at equilibrium. The bars above indicate the range of ligand concentrations tested in experiments. Each black line indicates a distinct parameter set. (C) Schematic of the finite differencing model. Diffusion was allowed within a radially symmetric region of interest. Peak Gas6 amount was held constant while varying spatial profiles of concentration. (D) Average and peak concentration for differing Gas6 spatial profiles. (E) Modeling output for AXL phosphotyrosine density at the peak point of Gas6 (r = 0) at 30 min with respect to varied Gas6 concentration profiles. Autocrine Gas6 levels and AXL expression were set to A549 levels. “D” indicates distinct diffusion coefficients specified in length units of the region of interest. (F) Modeling output for overall AXL phosphotyrosine under identical conditions. (G)~Modeling output of surface species abundance at 30 min under identical conditions.

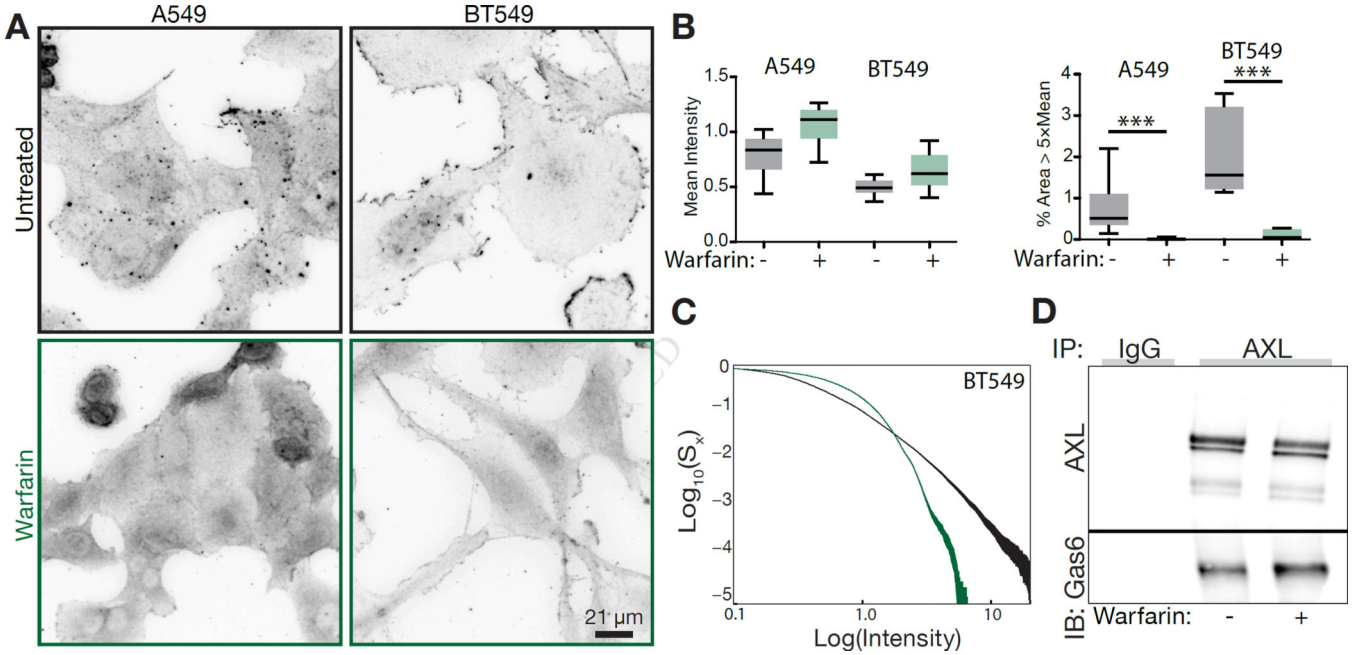

Figure 4. Spatially localized ligand presentation underlies robust autocrine AXL activation

(A) Immunofluorescence of AXL localization with or without warfarin treatment. (B) Quantification of mean AXL immunofluorescence intensity (left) and the fraction of pixels 5-fold above mean AXL intensity under each condition. (C) Cumulative distribution of AXL staining pixel intensities for BT549 cells with (green) or without (black) warfarin treatment. Both the intensity and remaining cumulative distribution density axes are presented on a log scale for ease of visualization. (D) Coimmunoprecipitation of AXL and Gas6 in MDA-MB-231 cells in the presence or absence of warfarin.

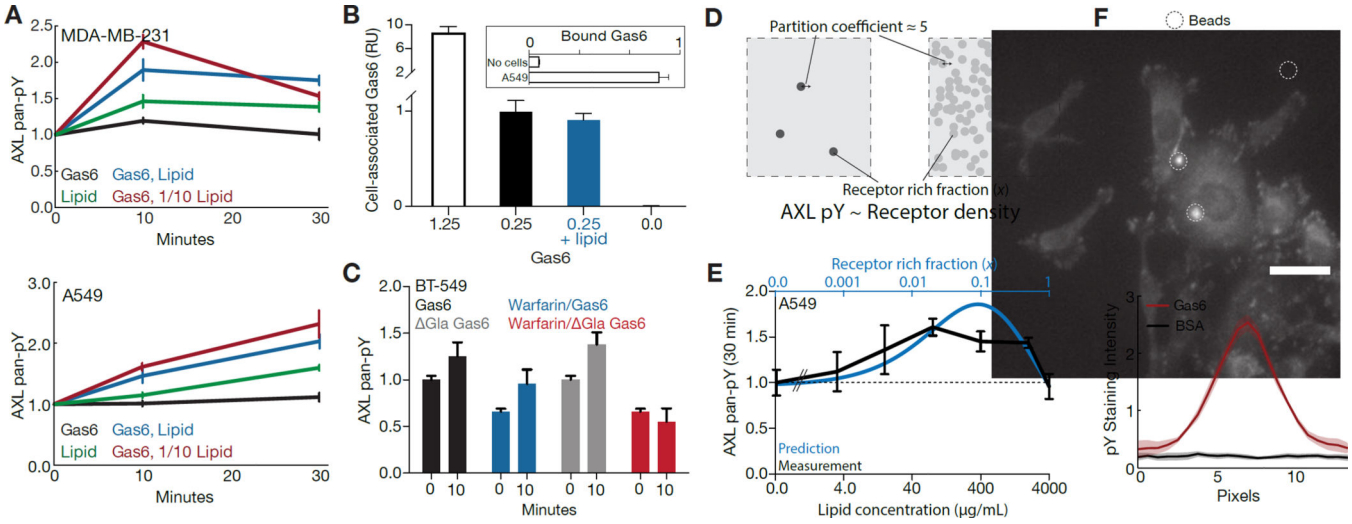

Figure 5. Validation of the spatial AXL signaling model

(A) Measurements of AXL pan-pY in MDA-MB-231 (top) and A549 (bottom) upon stimulation with PtdSer-containing vesicles in the presence of 0.25 nM Gas6. 1× and 1/10× lipid concentrations correspond to 100 μg/mL and 10 mg/mL of lipid, respectively. (B) Measurement of cell-associated Gas6 with A549 cells stimulated with Gas6 in the presence or absence of lipid. Inset shows amount of Gas6 quantified with or without cells present for the 1.25 nM Gas6 condition. (C) Measurement of AXL phosphorylation at 10 min in BT-549 cells in response to 1.25 nM Gas6 with or without warfarin pretreatment and with or without the Gla domain present in the exogenous ligand. (D) Diagrammatic explanation of the basis for a biphasic response with respect to lipid concentration. At low concentrations of PtdSer-containing lipid, receptor partitions into local regions resulting in robust activation. At very lipid concentrations PtdSer interaction is ubiquitous. Thus, even though receptor partitions into PtdSer-interacting regions this does not result in high local receptor density. E) Prediction and measurement of AXL phosphorylation at 30 min with varying amounts of PtdSer-containing vesicles and 0.25 nM Gas6. (F) Phosphotyrosine immunofluorescence (top) of MDA-MB-231 cells starved and stimulated with polystyrene beads coated with BSA or Gas6, and quantification of the immunofluorescence (bottom, N > 10). Cells were stimulated for 30 min prior to fixation. Error bars indicate the standard error of triplicate measurements, unless indicated otherwise.

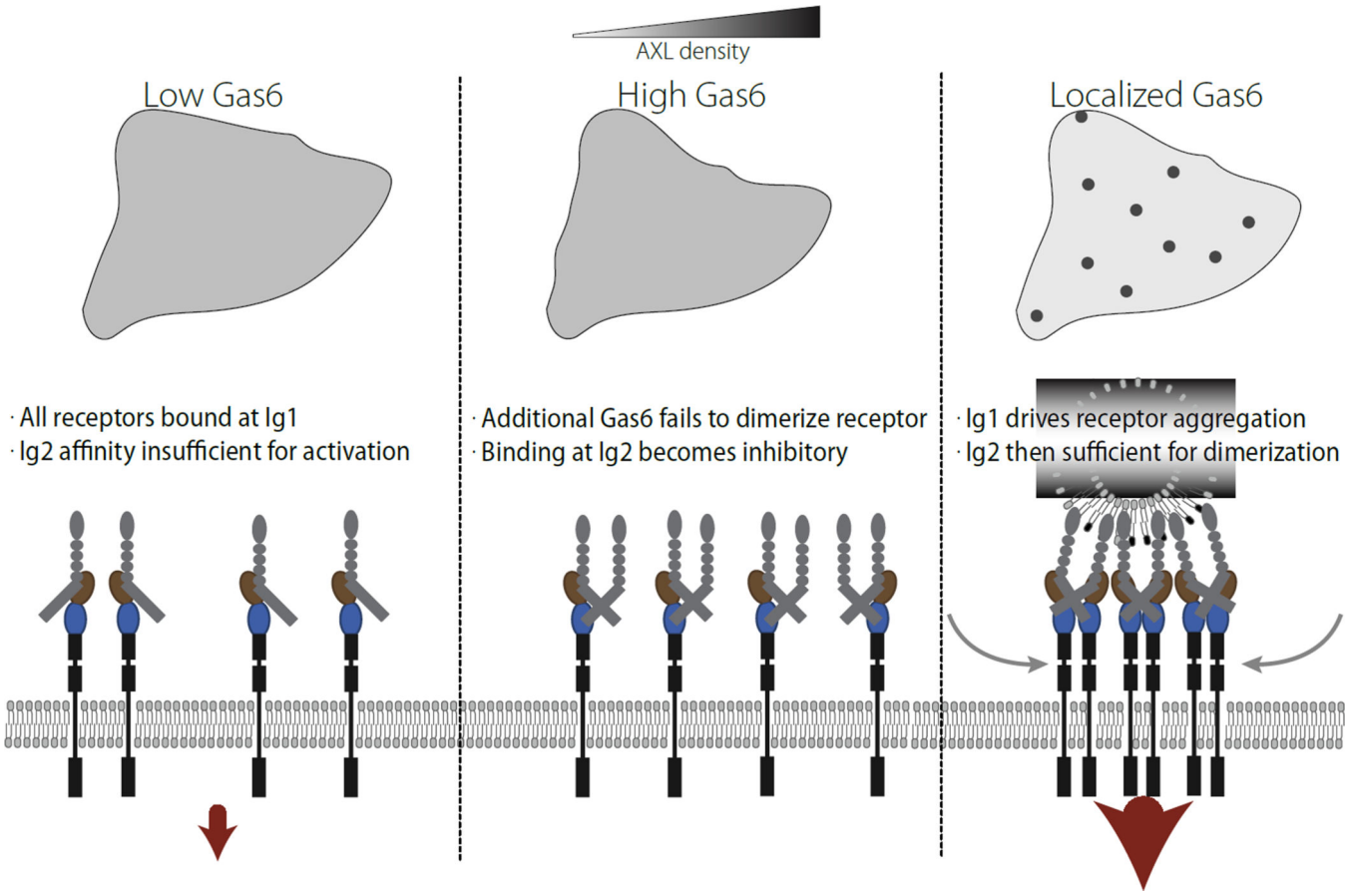

Figure 6. Model for efficient activation of AXL signaling

In the low Gas6 regime, the low affinity site is insufficient for receptor dimerization and activation by ligand. In the presence of a high, uniform concentration of Gas6, occupation of the low affinity site acts as a competitive inhibitor, since the A_{12} species is unable to dimerize with itself. Only with presentation of localized Gas6 is strong receptor activation observed, driven by diffusional influx of receptors from regions of low Gas6 concentration. This provides the appropriate localized signal for function of the receptor as a marker for PtdSer-exposure.